Zhang, W. *et al*. *Géotechnique* [https://doi.org/10.1680/jgeot.20.P.086]

Scale effects during cone penetration in spatially variable clays

WANGCHENG ZHANG*, YUTAO PAN† and FRASER BRANSBY‡

Cone penetration testing (CPT) has become one of the most commonly adopted in situ tests for site investigations, due to its reliability and repeatability of the measurements and the potential for direct use in design. For CPTs in clays, previous studies have paid considerable attention to the selection of penetration resistance factor N_{kt} considering the effects of soil stiffness, stress and strength anisotropy, soil layering and soil sensitivity, and so on. In contrast, this paper focuses on the effects of spatially variable soil properties on the interpretation and use of CPT data. This has been achieved using large-deformation finite-element modelling with random fields. It is shown that when using CPT data to obtain the true point-to-point statistics of the ground, scale effects could lead to the (unconservative) overestimation of the low estimate and underestimate of the high estimate for variable ground with small scales of fluctuation. Suggestions are made for correcting CPT-measured data to allow for this effect. In contrast, if using CPT data to provide design inputs for (larger) foundations, the same scale effects may be considered to increase beneficially the characteristic values of soil strength for sizing and reduce characteristic soil strengths for installation assessment.

KEYWORDS: clays; design; finite-element modelling; footings/foundations; shear strength; statistical analysis

INTRODUCTION

Cone penetration testing (CPT) has become one of the most commonly adopted in situ tests for site investigations, due to its reliability and repeatability of the measurements (Lunne *et al*., 1997). Cone penetrometers are cylindrical in shape with a conical tip, as shown in Fig. 1(a). A standard industry cone has an area of 1000 mm^2 (diameter, $D = 35{\cdot}7$ mm) with a 60° tip–apex angle, although 1500 mm^2 ($D = 43{\cdot}7$ mm) cones have been using increasingly for soft clays, especially for offshore applications (Randolph & Gourvenec, 2011). For offshore applications, CPT results are essential inputs in providing information about soil properties continuously with depth for foundation design and geohazard assessment (Lunne, 2012).

Cone penetrometer test data (mainly penetration tip resistance, sleeve friction and the excess pore pressure) have been used to provide information about soil identification (Robertson, 1990) and to quantify undrained shear strength (Lunne *et al*., 1997; Low *et al*., 2010) in undrained conditions (and relative density in drained conditions). In addition, CPT data have been used directly for foundation design (Sanglerat, 1972), particularly for the assessment of pile driving (e.g. Robertson *et al*., 1989) and axial pile capacity (e.g. Lehane *et al*., 2005; Van Dijk & Kolk, 2010 etc.).

In saturated clays, the standard cone penetration rate of 20 mm/s (ISO, 2014) does not permit the drainage of excess pore pressure and hence the cone tip resistance, q_c, can be related to the undrained shear strength, s_u, through a resistance factor, N_{kt}, by

$$s_u = \frac{q_c - \sigma_{v0}}{N_{kt}} = \frac{q_{net}}{N_{kt}} \quad (1)$$

where σ_{v0} is the total overburden stress and $q_{net} = q_c - \sigma_{v0}$ is the net cone tip resistance. q_c needs to be corrected in practice with respect to the net area ratio, which is not relevant in the numerical modelling in the current study. The value of N_{kt} can be estimated in theory by either closed-form solutions (such as the cavity expansion theory (Yu, 2000)) or numerical analyses (Ma *et al*., 2016), although in practice modifications to the selected N_{kt} value are often made based on site-specific calibration with laboratory strength tests. The value of N_{kt} has been shown to be affected by various soil characteristics – for example, soil stiffness, stress and strength anisotropy, soil layering and soil sensitivity – and a rough range of $N_{kt} \in (10, 14)$ with a mean of 12 in terms of the triaxial compression strength was reported by Low *et al*. (2010) based on a set of field penetration tests at several sites. Either the analytical solutions or the calibrations with parallel laboratory tests of soil samples from nearby sites require or assume the soil domain is homogeneous.

In reality, the ground or seabed is heterogeneous due to its complex sedimentation history and geological events since its formation (e.g. Phoon & Kulhawy, 1999). This is illustrated by the highly variable CPT data presented in Fig. 1(b), which show significant variations both vertically and horizontally. Previous studies on many onshore geotechnical applications such as shallow foundations, slopes and improved ground show that the spatial variability has an extensive impact on the global behaviour of geotechnical structures, hence influencing the choice of design values (Kasama *et al*., 2019; Pan *et al*., 2019, 2020; Zhu *et al*., 2019). For example, studies investigating the undrained bearing capacity of foundations in heterogeneous clays have revealed failure mechanisms (and bearing capacity factors) different from those in homogeneous ground, and that the mobilised undrained shear strength relies on the soil area that a foundation may mobilise and the soil strength variance within that zone of influence. Such effects have the potential also to affect the undrained shear strength measured using a CPT and how these

Manuscript received 13 March 2020; revised manuscript accepted 10 July 2020.
Discussion on this paper is welcomed by the editor.
* Oceans Graduate School, the University of Western Australia, Perth, WA, Australia (Orcid:0000-0001-9535-0211).
† Department of Civil and Environmental Engineering, Norwegian University of Science and Technology, Trondheim, Norway; formerly National University of Singapore, Singapore (Orcid:0000-0001-9504-1347).
‡ Oceans Graduate School, the University of Western Australia, Perth, WA, Australia (Orcid:0000-0001-8444-5995).

Downloaded by [Universitetsbiblioteket i Trondheim] on [25/08/20]. Copyright © ICE Publishing, all rights reserved.

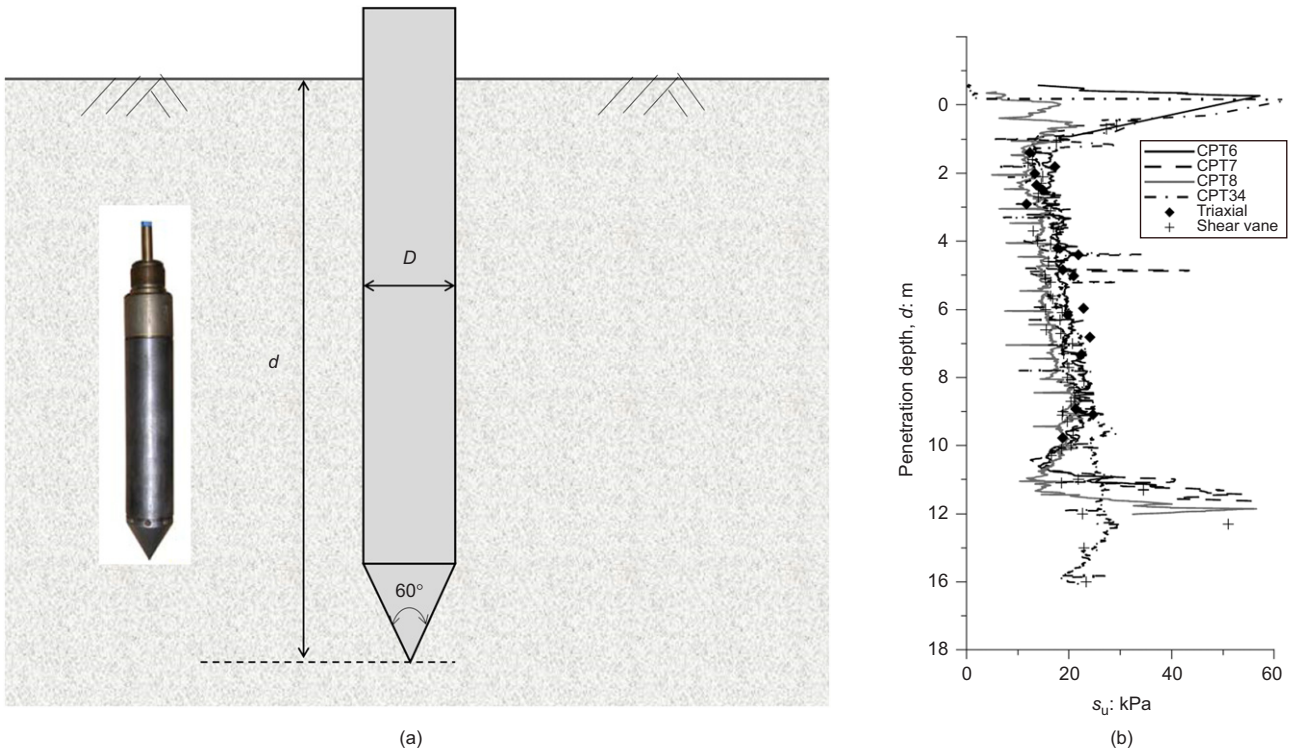

Fig. 1. (a) Cone penetrometer and schematic penetration; and (b) Ballina field CPT data (after Kelly *et al.*, 2017)

measured values relate to the global performance of a foundation in spatially variable clay. This is somewhat analogous to the soil layering effect (as discussed by Walker & Yu (2010), Bienen *et al.* (2015) and Ma *et al.* (2016), among others), whereby the undrained shear strength measured through a CPT does not directly relate to the bearing capacity of a foundation (e.g. during 'punch through' during penetration from strong to weak soils).

To investigate these effects, a series of cone penetration tests in heterogeneous soil have been modelled using a large-deformation finite-element (LDFE) analysis. The statistics of the resultant cone tip resistance (q_c) for different ground conditions have been quantified to investigate how the magnitude (coefficient of variation of point strength) and spatial correlation (scale of fluctuation (SOF) normalised by the cone diameter) affect the measured cone resistance and therefore the interpreted undrained shear strength. Finally, the direct use of CPT data for foundation design in heterogeneous soil is also addressed, based on better understanding of the effect of the soil spatial variability on penetration resistance.

LARGE-DEFORMATION RANDOM FINITE-ELEMENT MODELLING

Spatial variability of clays

The spatial variability is an inherent characteristic of marine clay formed by long-term geological actions such as tectonic movement and transport of sediment from various sources. It is usually modelled as a random field, the statistical properties of which can be concisely described using a mean, a coefficient of variation (COV) and a SOF with radial and vertical components denoted by δ_r and δ_z, respectively.

The typical reported values of COV and SOF of marine clays are listed in Table 1. The COV of marine clay ranges from 0·05 to 0·5. The horizontal SOF ranges from 5 to 50 m and is usually about an order of magnitude larger than the vertical SOF in marine clay. This is consistent with the layered pattern of marine clay formed by sedimentation.

The random fields of the point property were generated by the modified linear estimation method (MLEM) (Liu *et al.*, 2014). The statistical distribution of the undrained shear strength was a truncated Gaussian distribution with a mean value of 10 kPa. The undrained shear strength was truncated at 0·1 kPa to avoid occurrence of negative strength. In other studies, a lognormal distribution was widely used to rule out the occurrence of negative strength (e.g. Griffiths & Fenton, 2004; Huang & Griffiths, 2015; Tabarroki & Ching, 2019). The Monte Carlo approach was used to quantify the statistical properties of the outputs, whereby 100 separate LDFE realisations were conducted to reach convergent statistical values. The random (strength) fields were generated using a squared autocorrelation function

$$\rho(\Delta r,\ \Delta z) = \exp\left[-\pi(\Delta r/\delta_r)^2 - \pi(\Delta z/\delta_z)^2\right] \quad (2)$$

where Δr and Δz are radial and vertical distances from the point of interest. In this study, the radial SOF (δ_r) was fixed to be ten times the vertical SOF (δ_z) based on the information in Table 1. A similar ratio of horizontal SOF over vertical SOF can be found in previous studies (Li *et al.*, 2017; Yi *et al.*, 2020).

Numerical modelling details

A two-dimensional LDFE method with an axisymmetric model has been adopted, making use of the 'remeshing and interpolation technique with small strain' (RITSS; Hu & Randolph, 1998). RITSS is a category of arbitrary Lagrangian–Eulerian method, dividing the whole analysis into a series of small strain increments. In each increment, the Lagrangian formula is performed, and followed by remeshing based on the current configuration and interpolation of field variables from old to new meshes. Field variables include material properties, stresses and strains. An advantage of RITSS is that remeshing and interpolation can be

Downloaded by [Universitetsbiblioteket i Trondheim] on [25/08/20]. Copyright © ICE Publishing, all rights reserved.

Table 1. Summary of COVs and SOFs for soil shear strength parameters

Soil property	Soil type	Coefficient of variation	Scale of fluctuation: m		Reference
			Horizontal	Vertical	
s_u	Marine clay, Japan	—	—	1·3–2·7	Matsuo (1976)
s_u	New Liskeard varved clay	—	46	5·0	Vanmarcke (1977)
s_u	Dagang silty clay	—	—	0·56	Gao (1996)
s_u	Clay	0·1–0·5	—	0·8–6·1	Phoon & Kulhawy (1999)
s_u	Clay	—	—	0·25–2·5	Hicks & Samy (2002)
s_u	Sensitive clay, soft clay	—	20–80	2·0–6·0	El-Ramly *et al.* (2003)
s_u	Chicago clay	—	—	0·79–1·25	Xie (2009)
s_u, c, ϕ	In situ soils	—	30–60	1–6	Ji *et al.* (2012)
s_u(VST)	Clay	0·1–0·2	46–60	2·0–6·2	Phoon & Kulhawy (1999)
s_u(DST)	Clay	—	92·4	1·19–1·23	Ronold (1990)
$s_u(q_c)$	Clay	—	—	0·1–1·8	Cheng *et al.* (2000)
$s_u(q_c)$	Taranto clay	—	—	0·287–0·401	Cafaro & Cherubini (2002)
$s_u(q_c)$	Sand, clay	0·28	—	0·13–1·11	Uzielli *et al.* (2005)
$s_u(q_c)$	Tianjin port clay	—	8·37	0·132–0·322	Yan *et al.* (2009)
$s_u(q_c)$	Tianjin port muck and mucky clay	—	12·70	0·140–1·000	Yan *et al.* (2009)
$s_u(q_c)$	Tianjin port mucky clay and clay	—	10·77	0·158–0·568	Yan *et al.* (2009)
$s_u(q_c)$	Tianjin port mucky clay (sand inclusion)	—	6·53	0·159–0·319	Yan *et al.* (2009)
$s_u(q_c)$	Tianjin port silty clay	—	9·65	0·095–0·426	Yan *et al.* (2009)
$s_u(q_c)$	Silty clay	0·05–0·4	—	0·8–6·1	Haldar & Sivakumar Babu (2009)

Note: s_u, c, ϕ are undrained shear strength, cohesion and friction angle, respectively; s_u (VST) is undrained shear strength from vane shear test; s_u (DST), c (DST), ϕ (DST) are shear strength parameters from direct shear test; $s_u(q_c)$, $c(q_c)$, $\phi(q_c)$ denote the SOFs of shear strength parameters and are referred to those of cone tip resistance q_c from cone penetration test. '—' indicates data are not available.

conducted with any computing environment and programming language, coupled by a standard finite-element program. In this study, the Lagrangian calculations are fulfilled in the Abaqus platform (DSSC, 2014), while remeshing and interpolation processes are coded by Python and Matlab, respectively. Applications of RITSS on geotechnical engineering and its accuracy have been broadly addressed (e.g. Wang *et al.*, 2010, 2015; Zhou *et al.*, 2013; Zhang *et al.*, 2015).

The use of an axisymmetric model implicitly assumes that the two-dimensional property field is replicated along the axis of symmetry. In the random finite-element analysis with an axisymmetric model, the volumetric average of a soil property across each element is usually assigned to the element (Phoon *et al.*, 1990). However, such a volumetric average was not calculated in this study, because the average element size in the vicinity of the cone tip is much smaller than the SOFs, making the soil property within an element largely homogeneous.

There is a dilemma in the selection of mesh size for spatially variable ground. On one hand, the finite-element method mesh should be sufficiently small, with the correspondent maximum mesh size less than the SOF in each direction (Haldar & Mahadevan, 2000), to characterise the strength variation. On the other hand, mesh optimisation is necessary, with the mesh being denser in the zone of interest but coarser elsewhere to maintain computational efficiency. Specifically, when the CPT is initially at the shallow ground, the mesh is set to be relatively fine in the vicinity of the CPT (in shallow ground) but coarser far away from the CPT (deep). This gives the problem that the strength field may lose resolution in the deep zone and can never be recovered during the subsequent remeshing and interpolation processes, causing inaccuracy when the CPT approaches. To eliminate this problem, a set of dummy material points with sufficiently small intervals have been used in the spirit of the material point method to store the spatially varied material properties. After each increment, the positions of material points are updated with respect to the incremental displacement of the old mesh, and material properties are 'convected' from the updated material points to the integration points of the new mesh. The flowchart of the updated RITSS method is given in Fig. 2. Fig. 3 shows the finite-element model meshes and distributions of dummy material points for both shallow and deep penetration scenarios.

The piezocone model has a cone area of 1500 mm^2 (43·7 mm dia.) and a tip–apex angle of 60°. The sharp cone tip has been smoothed for better numerical convergence, as shown in Fig. 3. The soil ground is 32 times the cone diameter (32D) in both length and depth, with the central boundary (where the CPT crosses) allowed to move in the vertical direction only and the two outer boundaries fixed. Linear four-node rectangular elements with reduced integration were used. Mesh refinement at the cone tip is detailed in enlarged views on Fig. 3.

A Tresca yield criterion with an associated flow rule was used, which, in combination with Poisson's ratio of $\nu = 0{\cdot}495$, modelled soil behaviour in undrained conditions (i.e. ensuring very large bulk modulus at the elastic regime and zero volumetric strain in the plastic regime) as expected during cone penetration at the ISO standard rate (20 mm/s) in saturated clays.

The mean soil strength was set to $s_u = 10$ kPa at all depths. In reality, soil strength varies with depth depending on sedimentation history, stress history and the current effective stress profile. The effect of different strength gradients may be expected to change slightly the quantitative findings of this research, but not the overall conclusions. Consequently, a constant mean strength with depth was used as a simplifying first assumption.

A random strength field with spatial correlation is generated at the first increment of each realisation and stored at the material points, which move with the piezocone penetration as shown in Fig. 3. The initial spacing between material points is one-fortieth of the CPT diameter to guarantee sufficient strength resolution, which also corresponds with the minimum mesh size beneath the cone tip.

The soil shear modulus is $G \approx 100 s_u$ (or Young's modulus $E = 300 s_u = 2(1+\nu)G$) and hence the rigidity index $I_r \approx 100$. The submerged unit weight of soil was set to 7·85 kN/m^3 with the submerged soil density being 800 kg/m^3. These specific values are typical, with their exact values unlikely to affect the qualitative findings of the research significantly.

Downloaded by [Universitetsbiblioteket i Trondheim] on [25/08/20]. Copyright © ICE Publishing, all rights reserved.

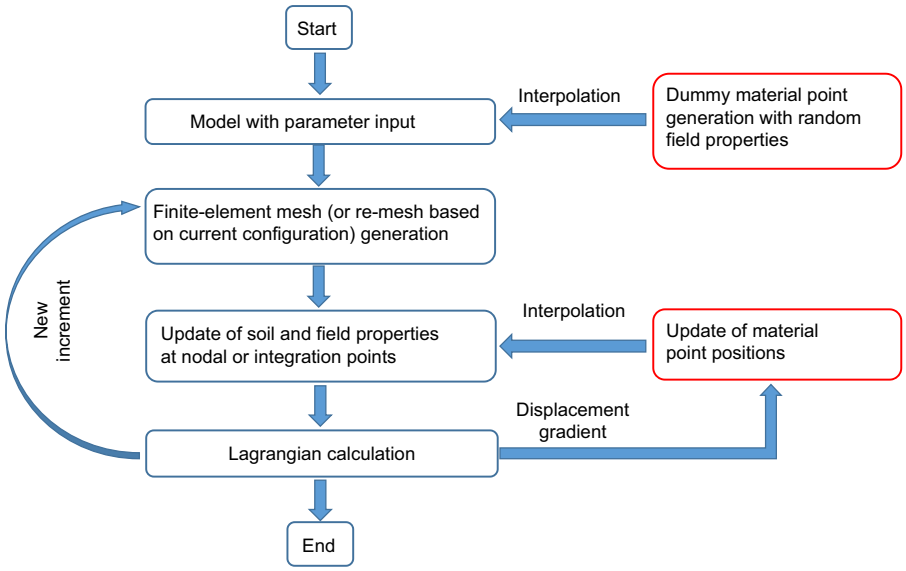

Fig. 2. Numerical modelling flowchart

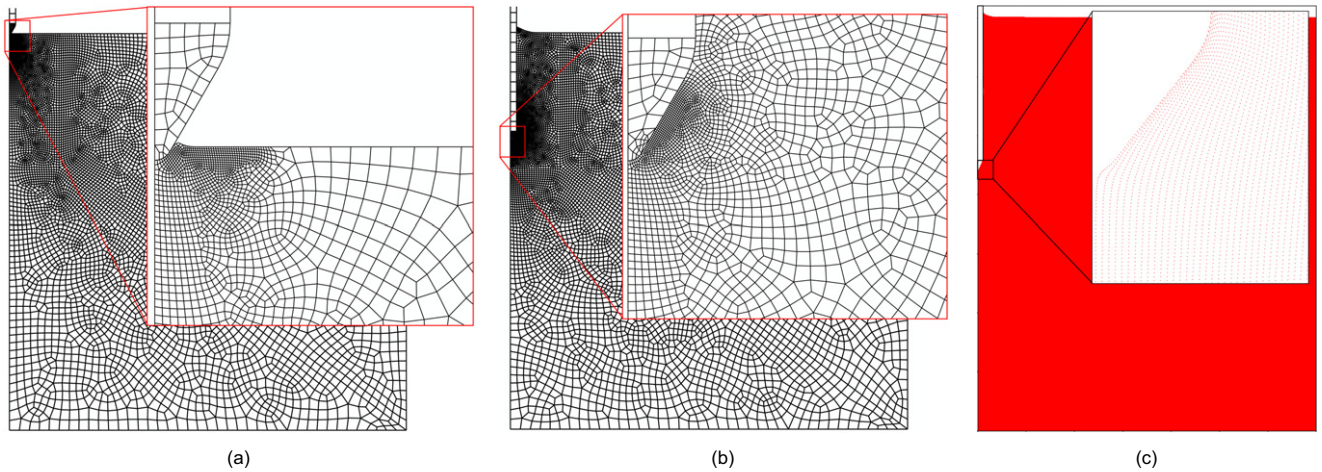

Fig. 3. (a) Finite-element model meshes for initial/shallow penetration; (b) finite-element model meshes for deep penetration; (c) dummy material points for random field storage (deep penetration)

Rather than penetrating from a certain depth (i.e. from a wished-in-place condition) as in many previously published small-strain analyses of the CPT, the analyses here started with the piezocone penetrating from the ground surface to a final depth 15D using LDFE modelling. In this way, both shallow and deep penetration conditions could be investigated.

Twenty different site conditions in terms of the soil strength (with different values of COV and/or SOFs) were investigated, each of which involved 100 realisations. Other parameters were kept the same, as shown in Table 2. In this study, δ_z was varied among 0·2D, 1D, 2D, 5D and 10D.

In addition to the above Monte Carlo analyses, an initial deterministic parametric analysis was conducted to investigate the effect of rigidity index on penetration resistance. This was used to validate the numerical approach against previously published solutions.

Table 2. Parameters for numerical modelling

Parameter	Value	Unit
Cone diameter, D	43·7	mm
Cone tip–apex angle	60	degrees
Overall ground length	1·4	m
Overall ground depth	1·4	m
Poisson's ratio, v	0·495	
Young's modulus, E	300 s_u	kPa
Undrained shear strength (mean), s_u	10	kPa
Submerged unit weight of soil	7·85	kN/m^3
Coefficient of variance, COV	0·1, 0·2, 0·3, 0·4	
Scale of fluctuation in vertical direction*, δ_z	8·74, 43·7, 87·4, 218·5, 437	mm

*Scale of fluctuation (SOF) in the radial direction δ_r is assumed to be 10 times the value of SOF in the vertical direction δ_z.

Comparison between axisymmetric and three-dimensional (3D) models

For axisymmetric problems in soils with only variations in depth, axisymmetric finite-element analyses are commonly performed. However, for a soil with spatially varying properties, axisymmetric analysis will not encapsulate the 3D distribution of the random field. Instead, a fully 3D analysis of the problem is required (Yi *et al.*, 2020). For the

Downloaded by [Universitetsbiblioteket i Trondheim] on [25/08/20]. Copyright © ICE Publishing, all rights reserved.

large-strain problem of a cone penetrating into a soil domain even a single axisymmetric analysis took 6 h of processing time (with a single central processing unit, using a normal desktop computer with a processor frequency of 3·4 GHz) and so a single set of 100 realisations (exploring one set of random field properties) required 600 h of calculations. Consequently, the much larger processing time required to perform such a set of calculations for 3D conditions would be prohibitive for current processor speeds. For example, approximately 48 h of processing time was required to penetrate a spudcan by 1·4 diameters using Abaqus 3D CEL modelling (Yi *et al.*, 2020). It is therefore necessary to assess whether such axisymmetric analysis will encapsulate the general properties of a 3D random field as it affects penetrometer resistance.

The above issue was investigated by performing vertical bearing capacity analyses of a wished-in-place pile for both axisymmetric and 3D random field conditions and comparing the results. Examples of random fields used in the axisymmetric and 3D analyses are shown in Figs 4(a)–4(c).

The dimensions of the pile and the clay properties are the same as the cone penetration tests except the cone tip is removed with only the cylinder (pile) left and the pile is wished in place at a depth of 8D. For simplicity, small-strain finite-element analyses were employed for both models with a limited additional penetration of 0·1D.

Figure 5 presents the results of deterministic analysis of a pile in a uniform strength soil zone from both 3D and axisymmetric analyses. The good agreement suggests that later non-deterministic comparison is valid.

The results from axisymmetric and 3D analyses are compared for two scenarios $\delta_z/D = 1$ and $\delta_z/D = 5$ with COV fixed at 0·3. The bearing capacity factor, N_c, is calculated at a displacement of 0·1D and compared as shown in Fig. 4(d). In both scenarios, the 3D mean value and COV of N_c is slightly (1–2% for the former and 5–15% for the latter) smaller than the axisymmetric results. The difference between the axisymmetric and 3D results may be attributed to the following.

(*a*) The horizontal SOFs (radial direction: $\delta_r = 10\delta_z$; circumferential direction: $\delta_\theta = \infty$) are much larger than the pile (cylinder) diameter (0·1–5 times δ_z), which is the case for most engineering applications. This in effect resembles a 3D random field in which the horizontal SOFs are much larger than the pile diameter ($\delta_x = \delta_y = 10\delta_z$), because both random fields are largely homogeneous in the horizontal directions in the vicinity of the pile tip.

(*b*) The circumferential strain in the 3D model is observed to be small (around 1/10 on average) compared to the radial strain, implying the 3D result can be approximated by the average of individual axisymmetric

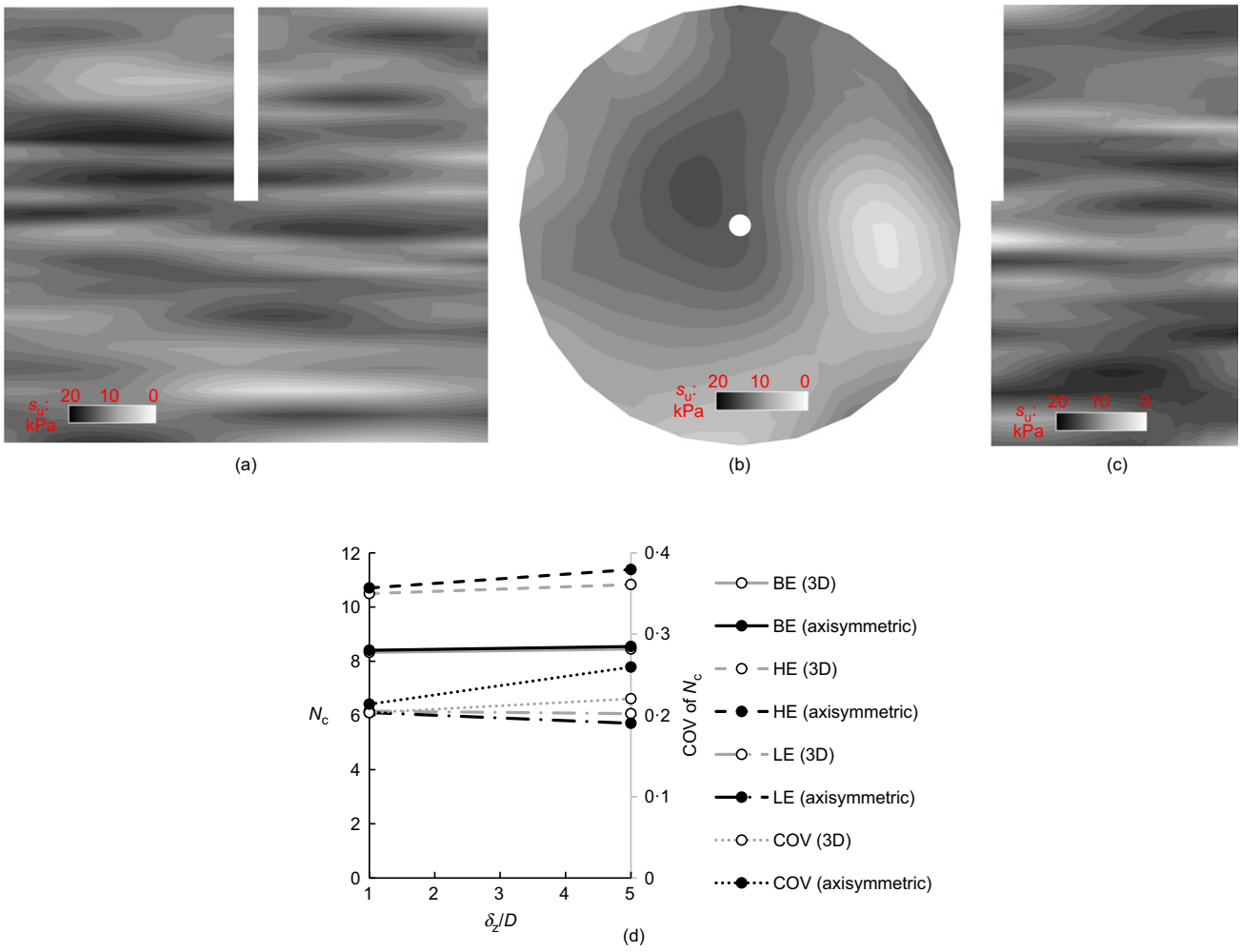

Fig. 4. Axisymmetric and 3D models of a wished-in-place pile: (a) vertical plane of a random field (COV = 0·3 and $\delta_z/D = 1$) in three dimensions; (b) top plane of a random field (COV = 0·3 and $\delta_z/D = 1$) in three dimensions; (c) a random field (COV = 0·3 and $\delta_z/D = 1$) in axisymmetric model; (d) comparison of N_c statistics for axisymmetric and 3D models (BE is the best estimate, or mean value; HE is the high estimate, or 90% fractile; LE is the low estimate, or 10% fractile; COVs of N_c correspond to the secondary axis)

Downloaded by [Universitetsbiblioteket i Trondheim] on [25/08/20]. Copyright © ICE Publishing, all rights reserved.

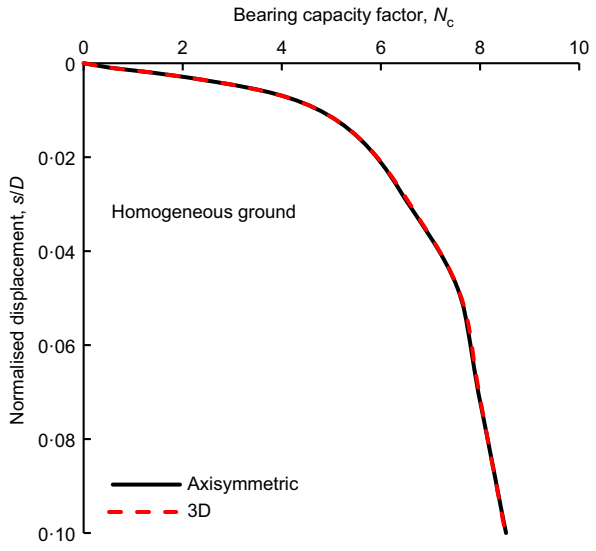

Fig. 5. Deterministic calculated N_c of a wished-in-place pile for axisymmetric and 3D analyses

results. As a result of the local averaging effect, the output COV of the 3D analysis is slightly lower than the axisymmetric counterpart.

RESULTS AND DISCUSSION

Deterministic analysis of CPT in homogeneous clay

A set of deterministic analyses of CPT penetration in homogeneous clay ($s_u = 10$ kPa) was carried out to compare the results against published results. The analysis was conducted to explore the effect of rigidity index $I_r = G/s_u$, which was varied between around 50, 100, 150, 200, 300 and 500.

Figure 6(a) shows the calculated penetration resistance factor, N_{kt}, according to equation (1) against the cone tip penetration depth (z) normalised by cone diameter (i.e. z/D). The value of N_{kt} approximately levels off at $z/D > 6$ when $I_r = 50$ or 100, where a deep penetration mechanism occurs, and the critical penetration depth for the deep mechanism increases with the increase of I_r. The deep penetration resistance factor is compared with a set of existing solutions, as shown in Fig. 6(b), including those from cavity expansion

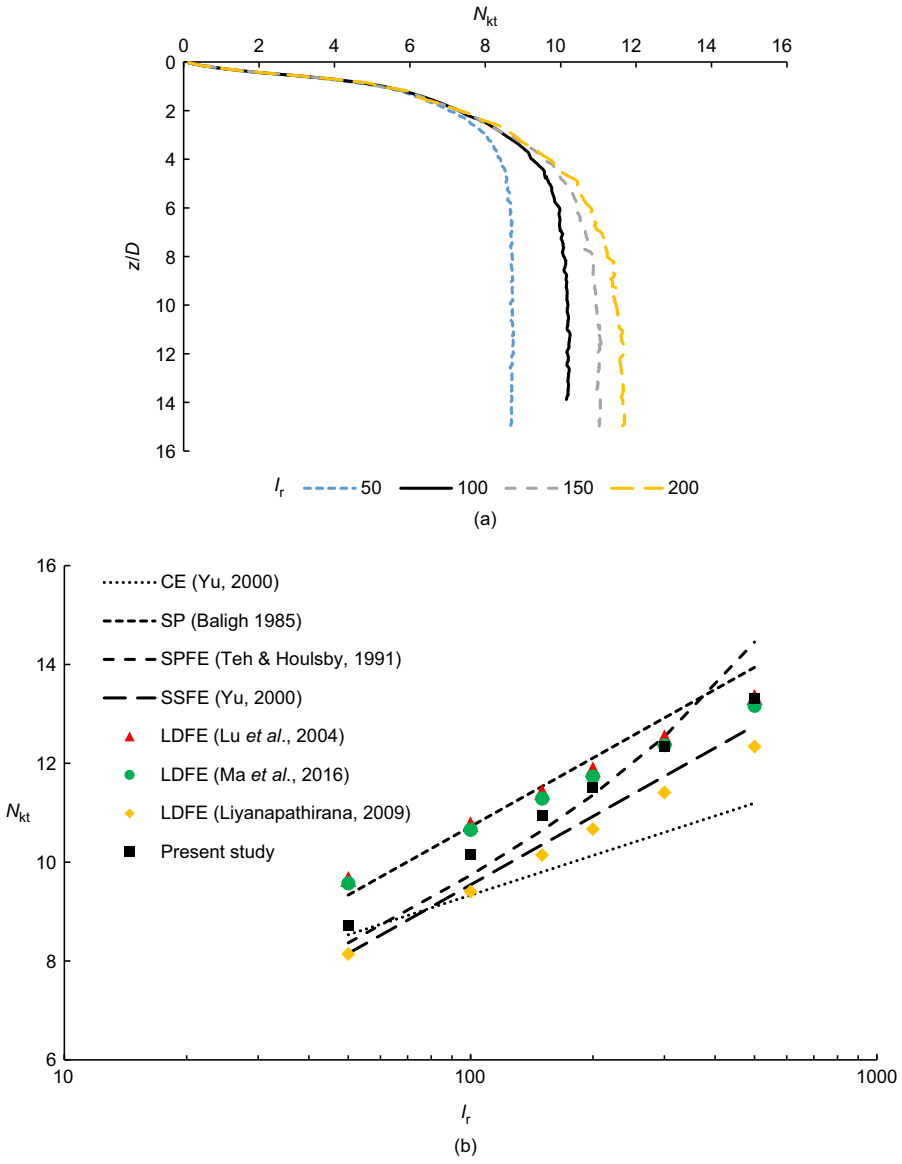

Fig. 6. Deterministic CPT data in homogeneous ground and comparison to existing solutions: (a) numerical resistance factors N_{kt} at different normalised depths z/D; (b) peak N_{kt} plotted against rigidity index I_r compared to existing solutions (CE, cavity expansion theory; SP, strain path method; SPFE, strain path finite-element analysis; SSFE, steady-state finite-element analysis)

Downloaded by [Universitetsbiblioteket i Trondheim] on [25/08/20]. Copyright © ICE Publishing, all rights reserved.

theory (Yu, 2000), strain path method (Baligh, 1985), strain path finite-element analysis (Teh & Houlsby, 1991), steady-state finite-element analysis (Yu, 2000) and LDFE analyses by Lu *et al.* (2004), Liyanapathirana (2009) and Ma *et al.* (2016).

Results from the current study fall near the mean of the previously published results, with a correlation between N_{kt} and I_r for a smooth cone given by

$$N_{kt} = 1{\cdot}13 + 1{\cdot}96\ln(I_r) \quad (3)$$

where the slope is close to the Baligh strain path solution and the steady-state finite-element analysis (= 2), and the intercept at $I_r = 1$ is lower than the Baligh strain path solution (= 1·51) but higher than other analytical solutions.

In the following random analysis, a fixed rigidity index, $I_r \approx 100$ (or $E = 300s_u$, where s_u is spatially variable with the mean of 10 kPa), was used with the deterministic penetration resistance factor being $N_{kt} = 10{\cdot}16$.

Example analysis of CPT in heterogeneous clay: deformation mechanisms and cone profiles

Figure 7 shows failure mechanisms at three selected penetration depths ($z/D = 2$, 6 and 10) for one homogeneous

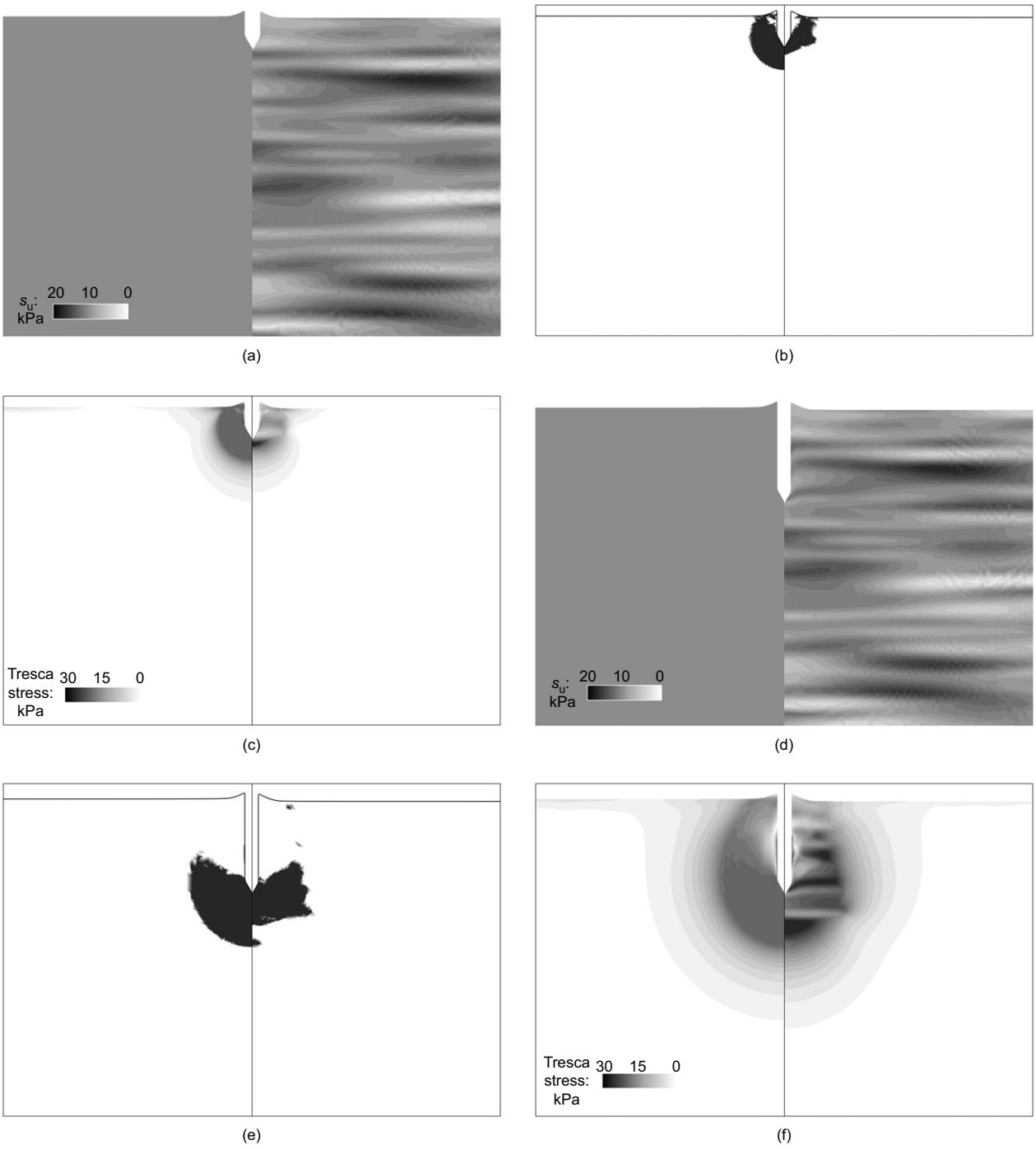

Fig. 7. A typical realisation of ground with spatially variable undrained shear strength compared with uniform ground: (a) undrained shear strength, (b) yield region and (c) Tresca stress for $z/D = 2$; (d) undrained shear strength, (e) yield region and (f) Tresca stress for $z/D = 6$; (g) undrained shear strength, (h) yield region and (i) Tresca stress for $z/D = 10$ (note the q_{net} curves represent typical penetration resistance profiles in homogeneous and heterogeneous grounds, respectively) (continued on next page)

Downloaded by [Universitetsbiblioteket i Trondheim] on [25/08/20]. Copyright © ICE Publishing, all rights reserved.

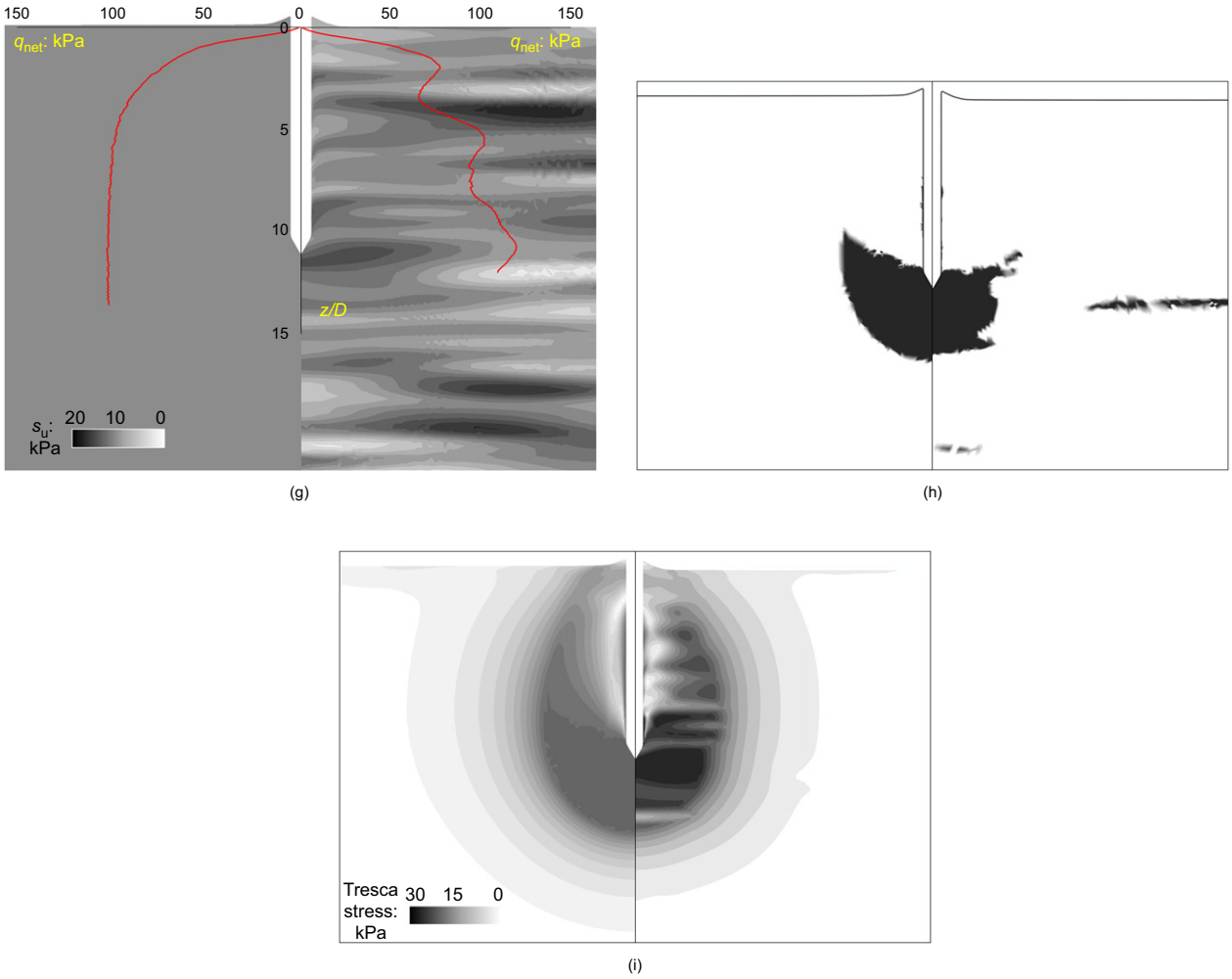

Fig. 7. Continued

analysis and one random analysis (i.e. a single realisation with COV = 0·3 and $\delta_z = 1D$). Shown in the figure parts are contours of soil strength, regions of plastic yielding and the maximum shear stress (or the Tresca stress, $(\sigma_1 - \sigma_3)/2$, where σ_1 and σ_3 denote the maximum and minimum principal stresses, respectively) in order to illustrate the effects of soil spatial variability on the instantaneous soil deformation mechanism. Fig. 7(g) also plots the net cone resistances, q_{net}, against the normalised penetration depth, z/D, for both the homogeneous and spatially variable analysis.

The transition between shallow and deep failure mechanisms can be identified in both the deterministic and spatially variable analysis. When the penetration depth is at $2D$, yield regions develop from the cone tip to the ground surface, indicating an unconstrained (i.e. shallow) failure mechanism. When the penetration depth is $6D$ or greater, however, 'butterfly' yield regions are concentrated around the cone tips, showing a constrained (i.e. deep) failure mechanism.

The plastic failure mechanism for shallow penetration resembles a shallow (unconfined) mechanism with a uniform concave outer slip line propagating to the ground surface, while the mechanism becomes non-uniform in the spatially variable ground, as shown in Fig. 7(b). The latter phenomenon is attributed to the deformation 'preferring' to propagate through weaker soils (to minimise the overall energy dissipation and therefore the cone resistance), and implies a different penetration resistance factor in the spatially variable case. Similarly, with deep penetration, the existence of weak soils in the spatially variable ground alters the deep mechanism, with the spatially variable mechanism mobilising soil further from the cone tip than in the homogeneous case. The net cone resistance varies with the alternate occurrence of weak and strong soils in the spatially variable ground rather than levelling off when the deep mechanism is mobilised as in the homogenous case, as illustrated in Fig. 7(g).

*Statistical distributions of CPT-measured undrained shear strength for the base case condition (*COV = 0·3 *and* $\delta_z = 1D$*)*

The undrained shear strength can be calculated directly from the tip resistance by way of equation (1), assuming that N_{kt} is a constant value (of 10·16 here, based on $I_r = 100$ and a smooth cone). This undrained shear strength is hereafter termed the 'CPT-measured' undrained shear strength and will reflect the soil strength and deformation occurring around the cone tip, rather than equalling the point value of undrained shear strength at the instantaneous position of the cone tip.

Figure 8(a) shows the results of 100 LDFE realisations with random spatial variability with COV = 0·3 and $\delta_z/D = 1$. Each realisation shows significant fluctuations with depth, resembling real CPT data, and there are significant differences between realisations. The CPT-measured strengths at each depth were analysed statistically to generate profiles of best estimate (BE, mean value), high estimate (HE, 90% fractile) and low estimate (LE, 10% fractile) strength. It should be noted that the estimates conform to offshore

Downloaded by [Universitetsbiblioteket i Trondheim] on [25/08/20]. Copyright © ICE Publishing, all rights reserved.

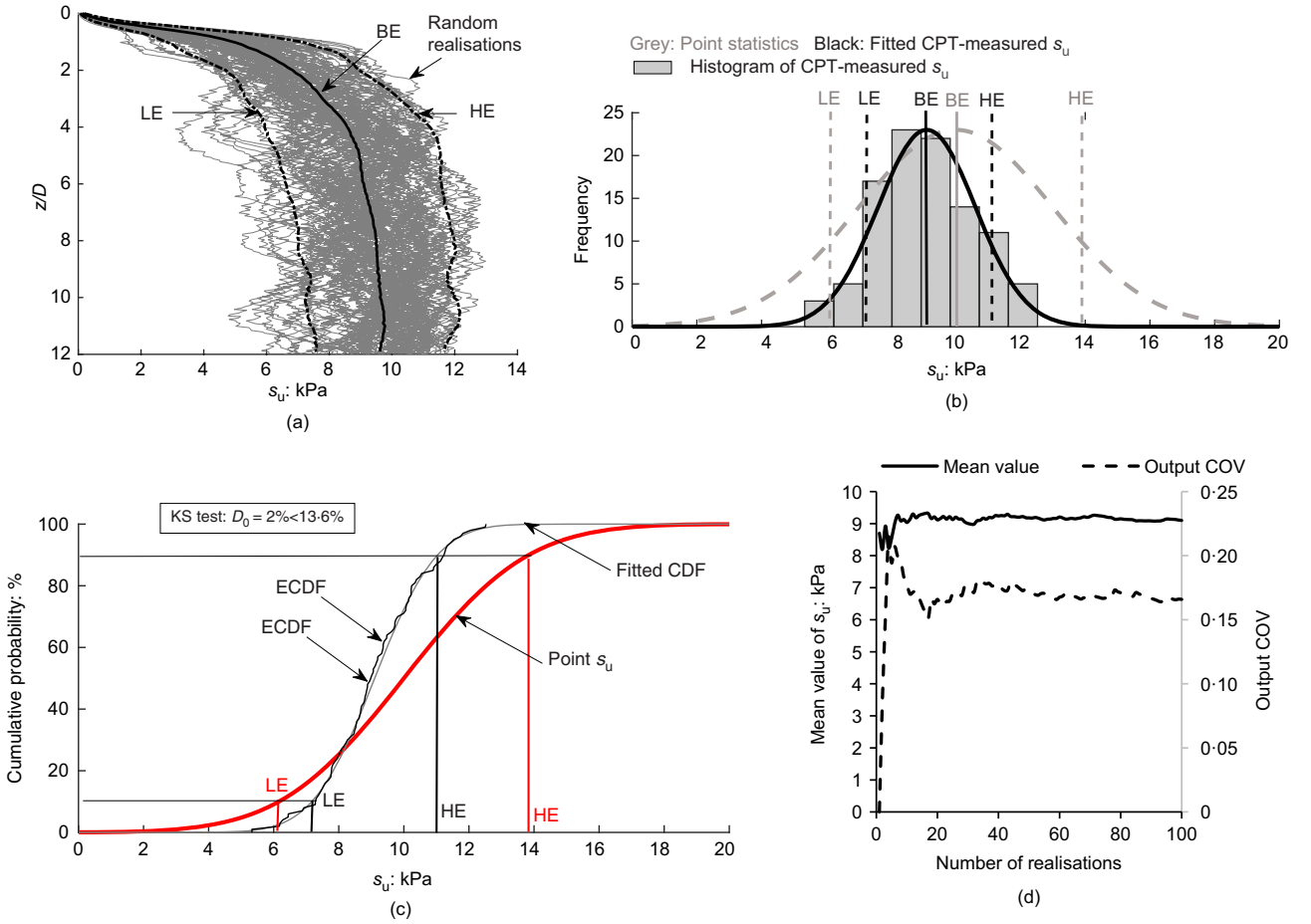

Fig. 8. Measured undrained shear strength s_u using deterministic penetration resistance factor N_{kt} = 10·16 for a typical case: (a) s_u plotted against normalised penetration depth z/D with 100 realisations; (b) histogram of s_u; (c) cumulative distribution of s_u (the goodness-of-fit test was conducted using Kolmogorov–Smirnov (KS) test, D_0 is the maximum vertical distance between the empirical cumulative distribution function (ECDF) and the cumulative distribution function (CDF). The value of 13·6% is the critical value of KS test for a sample with size 100 at significance level 0·05); (d) convergence plot of mean value and output COV of CPT-measured s_u

practice in which an 80% confidence interval is often used. This is different from the definition of characteristic values in Eurocode 7 (BS EN 1997-2 (BSI, 2007)), which usually use a 90% confidence interval (5% and 95% fractiles). Assessment for any specified confidence interval will be formulated and discussed later, as shown in equations (4) and (6). The BE is often defined as the median value, but it is expected to equal the mean here because a near-normal distribution of point strength was used. Fig. 8(d) shows that the mean value and output COV generally converge within 100 realisations.

The calculated CPT-measured undrained shear strengths for all realisations with $z/D > 6$ (i.e. where 'deep' conditions were encountered) were collected, and a histogram and cumulative distribution (calculated from a fit to the histogram) is plotted in black in Figs 8(b) and 8(c), respectively. Also shown in Figs 8(b) and 8(c) are the input – namely, the point distributions of undrained shear strength. A comparison of the empirical histogram of CPT-measured undrained shear strength and the probability distribution of point undrained shear strength shows that the former has a lower mean value and less scatter. This is consistent with previous studies on bearing capacity of a shallow foundation resting on spatially variable soils (Fenton & Griffiths, 2002; Hicks & Sammy, 2002; Hicks & Spencer, 2010; Hicks *et al.*, 2014; Shi *et al.*, 2020). There are two competing factors: the spatial averaging effect and the weakest path mechanism. Spatial averaging reduces the scatter of cone resistance (to close to the BE value). The latter potentially makes the BE below the mean value of point strength. The two effects combine to reduce the scatter in CPT-measured s_u and reduce the BE value, thereby leading to a higher LE and a lower HE CPT-measured s_u than for the (point-to-point) s_u input.

Effect of COV and SOF on statistical distributions of CPT-measured undrained shear strength

Figure 9 shows the Monte Carlo LDFE calculated LE (P10), BE (mean and P50) and HE (P90) values of 'CPT-measured' undrained shear strength (for $z/D > 6$) for different δ_z and input COV values.

Figure 9(a) shows that when the δ_z becomes far greater than the cone diameter the BE approaches the input mean value and the LE and HE tend towards the input P10 and P90 point s_u values. However, when the SOF is reduced, the BE value of CPT-measured resistances reduces a little (presumably because of the weakest path mechanism) and the HE to LE scatter of measured resistance reduces significantly (because of the local averaging effect). The net outcome is that the CPT-measured HE and BE are lower than the inputs and the LE value is higher than that of the input s_u distribution.

Figure 9(b) shows how the CPT-measured distributions of undrained shear strength are affected by the COV of the input strength distribution (for a fixed $\delta_z/D = 1$). The CPT-measured BE reduces with increasing input COV of point strength and is lower than the (fixed) point value when COV > 0. This is mainly because the failure mechanism attached to CPT penetration is dominated by the strength of weak zones instead of the mean strength, as discussed before. At

Downloaded by [Universitetsbiblioteket i Trondheim] on [25/08/20]. Copyright © ICE Publishing, all rights reserved.

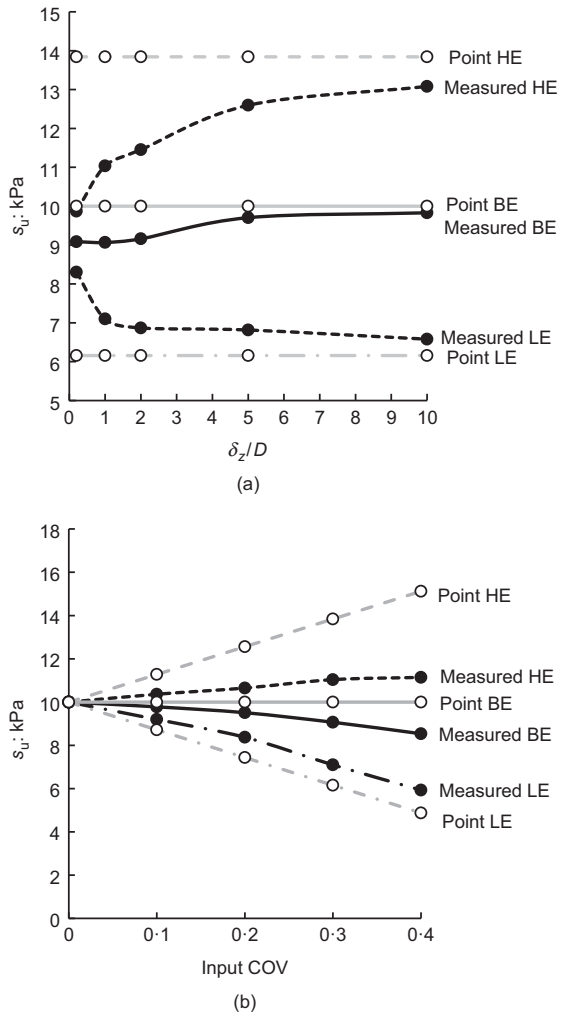

Fig. 9. Measured undrained shear strength s_u at $z/D > 6$ using deterministic $N_{kt} = 10{\cdot}16$ with respect to the effect of (a) SOF (δ_z) (for COV = 0·3) and (b) COV (for $\delta_z/D = 1$)

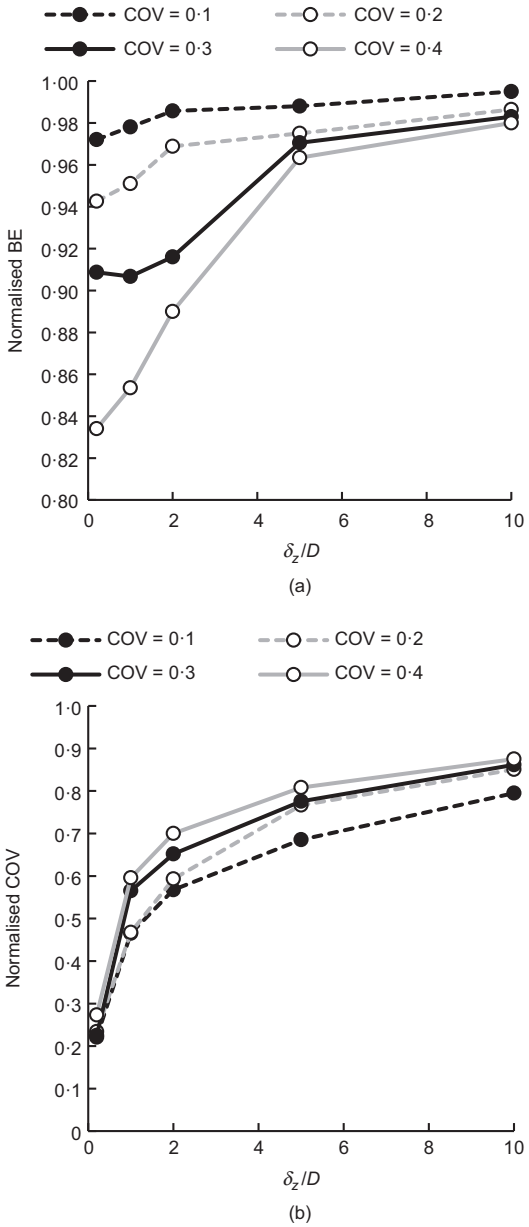

Fig. 10. (a) Normalised BE and (b) normalised output COV of measured undrained shear strength in terms of the input point values (e.g. the best estimate of CPT-measured strength is normalised by the best estimate of the point statistics)

the same time the HE to LE range reduced compared to point values. Consequently, the CPT-measured LE becomes greater than the input and the difference becomes significant with the increase of input COV, leading to more optimistic estimations. In contrast, the HE gradually increases with the increase of the input COV.

The same data are replotted in Figs 10 and 11, where the CPT-measured BE and its COV, LE and HE are normalised by the input point statistics. As expected, the normalised BE is less than unity, indicating it is underestimated for small values of δ_z and large values of COV, and increases with δ_z and reduces with input COV. The normalised output COV decreases with reducing δ_z (and increases with input COV), with the values at large δ_z/D approaching unity, as explained before. The normalised LE can be as high as 1·5 at $\delta_z/D = 0{\cdot}2$ and input COV = 0·4, and generally decreases towards unity with δ_z/D, but increases with input COV. Simultaneously, the normalised HE can be as low as 0·63 at $\delta_z/D = 0{\cdot}2$ and input COV = 0·4, and increases to unity with increasing δ_z/D, but appears to decreases with input COV. The normalised values of LE, BE, HE and COV at very large values of δ_z/D are expected to be unity.

SUMMARY OF FINDINGS AND IMPLICATIONS FOR DESIGN

The above discussion shows that direct use of the statistics of cone tip resistance in a spatially variable soil will underestimate the BE and HE s_u and overestimate the LE s_u compared to the 'real' (i.e. point-to-point population) statistics when $\delta_z/D < 20$. This has the potential to lead to inaccurate and potentially unsafe design practice. For example, the LE is usually adopted for a slope stability analysis, and an overestimation of LE produces a higher factor of safety than in reality. Therefore, in order to quantify the 'true' soil conditions (i.e. the statistics of the point-to-point soil strength), it may be necessary to make adjustments to the measured cone values. A method to do this with knowledge of the input COV and δ_z of the soil is given below.

(*a*) First calculate the statistical distribution of the CPT-measured shear strength to define the mean and standard deviation.
(*b*) Increase the cone-measured BE by the inverse of the normalised BE in Fig. 10(a), according to the

Downloaded by [Universitetsbiblioteket i Trondheim] on [25/08/20]. Copyright © ICE Publishing, all rights reserved.

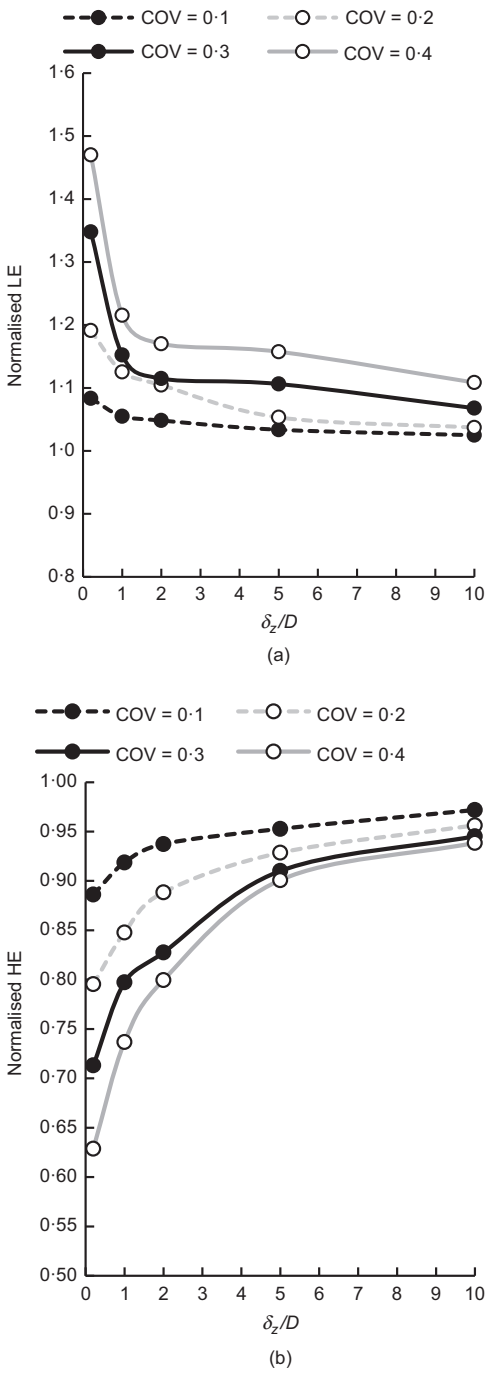

Fig. 11. (a) Normalised LE and (b) normalised HE of measured undrained shear strength in terms of the input point values (the low and high estimates of CPT-measured strength are normalised by the low and high estimates of the point statistics, respectively)

site-specific value of COV and the SOF of the soil. The adjusted BE of point statistics is denoted as BE_{adj}.

(*c*) Modify the CPT-measured COV to the point-to-point COV ('δ_{adj}') using Fig. 10(b) in the same way.

(*d*) Evaluate the low estimate of the adjusted point statistics (LE_{adj}) using

$$LE_{adj} = BE_{adj}(1 - \beta\delta_{adj}) \quad (4)$$

where β is the reliability index (BSI, 2002), which depends on the target probability of occurrence of worse cases (p) selected by the designer, as opposed to a calculated level of reliability in reliability analysis, and

$$\beta = -\Phi^{-1}(p) \quad (5)$$

where Φ is the cumulative distribution function of the standard normal distribution. For example, as LE is selected as the 10% fractile in the study (i.e. the P10 value of s_u), the value of β used is 1·281.

(*e*) Evaluate the high estimate of the point statistics (HE_{adj}) using

$$HE_{adj} = BE_{adj}(1 + \beta\delta_{adj}) \quad (6)$$

Whether the above adjustment is required depends on the COV of the soil and its known or expected SOF compared to the cone diameter. Given that significant deviation from the point statistics is only observed when $\delta_z/D < 20$, adjustment may only need to be applied to cases when $\delta_z < 0{\cdot}7$ m (for a standard 10 cm^2 cone) or $\delta_z < 0{\cdot}87$ m (for an enlarged cone). As the vertical SOF δ_z of the undrained strength of clays usually ranges between 0·1 and 6 m, this correction may not be required in the majority of seabed conditions.

IMPLICATIONS OF RESULTS FOR CPT-BASED FOUNDATION DESIGN

If using the cone-measured strengths to design a pile, the scale effects shown in Figs 9–11 will be relevant whether the design involves selecting representative strengths or using the cone data directly. If the CPT data are used directly in foundation design, they may overestimate the output COV and the BE of representative strengths because the spatial averaging and weakest path mechanisms are more significant owing to the large pile size compared to the cone. This would mean that the LE from the CPT interpretations may underestimate the values involved in foundation scales (potentially leading to design of a larger pile than required) and the HE would be an overestimate (generating unnecessarily onerous installation conditions). There is therefore likely to be significant design benefit in considering these scale effects in design.

The above scale effect can be accounted for by adjusting the CPT-measured data using Figs 10 and 11. This is illustrated using a worked example for a pile of diameter, $D = 2$ m in a soil with COV = 0·3 and $\delta_z = 2$ m (well within the range listed in Table 1). For the pile $\delta_z/D = 1$, whereas for the cone $\delta_z/D \approx 46$. For this case, the high δ_z/D value means that the CPT data represent the point strengths very well. However, the value of $\delta_z/D = 1$ indicates that according to Figs 10 and 11 the BE, LE and HE of representative strengths involved in foundation behaviours are 0·9, 1·15 and 0·80 of the values from the CPT interpretations, respectively. Consequently, the LE design line to calculate for pile end bearing resistance obtained from the cones should be increased by 15% (resulting in a smaller pile) and the HE design line for calculating soil resistance to driving might be reduced by 20% (which could result in faster installation or the requirement for a lower capacity installation device). Clearly, the knowledge of scale effects in spatially variable grounds revealed here may help to achieve more economic foundation designs.

CONCLUSIONS

The paper has investigated how tip resistance during CPTs in spatially variable clays is affected by the characteristics of the spatial variability. This has been achieved using LDFE analyses and by performing multiple realisations of different random soil strength fields using a Monte Carlo approach. The LDFE simulations were performed based on the RITSS (Hu & Randolph, 1998), with the result validated against previously published solutions for uniform soil conditions.

Downloaded by [Universitetsbiblioteket i Trondheim] on [25/08/20]. Copyright © ICE Publishing, all rights reserved.

The seabed variability in the LDFE simulations was modelled using a normal distribution of point strength with different selected COV values and different radial and vertical SOF values (δ_r and δ_z with the ratio δ_r/δ_z fixed as 10) in an axisymmetric soil domain. For all analyses, a smooth cone was simulated and the soil was modelled as elastic–perfectly plastic with a rigidity index (G/s_u) of 100. Despite the above limitations to the analysis, it is believed that the results highlight general statistical behaviour which will apply for other cone roughness values, soil constitutive laws and soil properties distributions.

The main findings are summarised as follows.

(*a*) The failure mechanisms in spatially variable grounds at both shallow and deep penetration depths are different from that in homogeneous ground. With deep penetration, the existence of weak soils in spatially variable ground alters the deep (cavity-expansion type) mechanism, which is usually larger than the homogeneous case. The phenomena may be attributed to the deformation preferring to propagate through weaker soil in the vicinity of the cone tip. As a consequence, the net cone resistance varies with the alternating occurrence of weak and strong soils in the spatially variable ground rather than levelling off at deep ground as in the homogeneous case.

(*b*) Generally, interpretations from CPT data give an underestimation of the BE and HE of undrained shear strength, but an overestimation of the LE. The difference between the CPT-measured and realistic strengths becomes more significant with the increase of the soil variance (related to COV) or the decrease of the length of the soil correlation (related to δ_z). For most cases, the value of δ_z is much larger than the cone diameter (D) and the deviation of undrained shear strengths interpreted from CPT data from the realistic values is minimal. However, for some extreme cases with very low δ_z ($<0{\cdot}5$ m), such that $\delta_z/D < 20$, the CPT-measured BE and HE need to be increased, while the LE may need to be decreased to represent the statistics of the point strengths. A method for adjustment of CPT-measured undrained shear strengths has been provided.

(*c*) The scale effect in terms of δ_z/D is more significant when subjected to the application of CPT data to foundation design, as dimensions of foundations are much larger and comparable to δ_z. Consequently, if the CPT-measured data are used directly in foundation design, the BE and HE from CPT data may be larger than applicable for a foundation, while the LE is underestimated. This implies that consideration of this effect may be used to modify CPT-measured data in order to achieve more economic foundation design.

ACKNOWLEDGEMENTS

The work presented in this paper is part of the research activities undertaken by the Centre for Offshore Foundation Systems within the Oceans Graduate School at the University of Western Australia. The third author holds the Fugro Chair in Geotechnics, whose support is gratefully acknowledged.

NOTATION

BE_{adj} adjusted best estimate of undrained shear strength (kPa)
D diameter (m)
E Young's modulus (kPa)
G shear modulus (kPa)
HE_{adj} adjusted high estimate of undrained shear strength (kPa)
I_r rigidity index
LE_{adj} adjusted low estimate of undrained shear strength (kPa)
q_c resultant cone tip resistance (kPa)
q_{net} net tip resistance (kPa)
s_u undrained shear strength (kPa)
β reliability index
Δr incremental radial coordinate (m)
Δz incremental vertical coordinate (m)
δ_θ circumferential scale of fluctuation (m)
δ_{adj} adjusted coefficient of variation (m)
δ_r radial scale of fluctuation (m)
δ_x scale of fluctuation in x-direction (m)
δ_y scale of fluctuation in y-direction (m)
δ_z scale of fluctuation in z-direction (m)
ν Poisson's ratio
ρ correlation
σ_{v0} total overburden stress (kPa)

REFERENCES

Baligh, M. M. (1985). Strain path method. *J. Geotech. Engng* **111**, No. 9, 1108.

Bienen, B., Qiu, G. & Pucker, T. (2015). CPT correlation developed from numerical analysis to predict jack-up foundation penetration into sand overlying clay. *Ocean Engng* **108**, 216–226.

BSI (2002). BS EN 1990:2002: Eurocode. Basis of structural design. London, UK: BSI.

BSI (2007). BS EN 1997-2:2007: Eurocode 7. Geotechnical design. Ground investigation and testing. London, UK: BSI.

Cafaro, F. & Cherubini, C. (2002). Large sample spacing in evaluation of vertical strength variability of clayey soil. *J. Geotech. Geoenviron. Engng* **128**, No. 7, 558–568.

Cheng, Q., Luo, S. X. & Gao, X. Q. (2000). Analysis and discussion of calculation of scale of fluctuation using correlation function method. *Chin. J. Rock Soil Mech.* **21**, No. 3, 281–283 (in Chinese).

DSSC (Dassault Systems, Simulia Corp) (2014). *Abaqus version 6.14 documentation*. Providence, RI, USA: DSSC.

El-Ramly, H., Morgenstern, N. R. & Cruden, D. M. (2003). Probabilistic stability analysis of a tailings dyke on presheared clay shale. *Can. Geotech. J.* **40**, No. 1, 192–208.

Fenton, G. A. & Griffiths, D. V. (2002). Probabilistic foundation settlement on spatially random soil. *J. Geotech. Geoenviron. Engng* **128**, No. 5, 381–390.

Gao, D. Z. (1996). Safety index of geotechnical design and its application. *Chin. J. Geotech. Investigation Surveying* **1**, 1–6 (in Chinese).

Griffiths, D. V. & Fenton, G. A. (2004). Probabilistic slope stability analysis by finite elements. *J. Geotech. Geoenviron. Engng* **130**, No. 5, 507–518.

Haldar, A. & Mahadevan, S. (2000). *Reliability assessment using stochastic finite element analysis*. Hoboken, NJ, USA: John Wiley & Sons.

Haldar, S. & Sivakumar Babu, G. L. (2009). Design of laterally loaded piles in clays based on cone penetration test data: a reliability-based approach. *Géotechnique* **59**, No. 7, 593–607, https://doi.org/10.1680/geot.8.066.3685.

Hicks, M. A. & Samy, K. (2002). Influence of heterogeneity on undrained clay slope stability. *Q. J. Engng Geol. Hydrogeol.* **35**, No. 1, 41–49.

Hicks, M. A. & Spencer, W. A. (2010). Influence of heterogeneity on the reliability and failure of a long 3D slope. *Comput. Geotech.* **37**, No. 7–8, 948–955.

Hicks, M. A., Nuttall, J. D. & Chen, J. (2014). Influence of heterogeneity on 3D slope reliability and failure consequence. *Comput. Geotech.* **61**, 198–208.

Hu, Y. & Randolph, M. F. (1998). A practical numerical approach for large deformation problem in soil. *Int. J. Numer. Analyt. Methods Geomech.* **22**, No. 5, 327–350.

Huang, J. & Griffiths, D. V. (2015). Determining an appropriate finite element size for modelling the strength of undrained random soils. *Comput. Geotech.* **69**, 506–513.

ISO (International Organization for Standardization) (2014). ISO 19901-8: Petroleum and natural gas industries – Specific

Downloaded by [Universitetsbiblioteket i Trondheim] on [25/08/20]. Copyright © ICE Publishing, all rights reserved.

requirements for offshore structures – Part 8: Marine soil investigations. Geneva, Switzerland: ISO.

Ji, J., Liao, H. J. & Low, B. K. (2012). Modeling 2-D spatial variation in slope reliability analysis using interpolated auto-correlations. *Comput. Geotech.* **40**, 135–146.

Kasama, K., Whittle, A. J. & Kitazume, M. (2019). Effect of spatial variability of block-type cement-treated ground on the bearing capacity of foundation under inclined load. *Soils Found.* **59**, No. 6, 2125–2143, https://doi.org/10.1016/j.sandf.2019.11.007.

Kelly, R. B., Pineda, J. A., Bates, L., Suwal, L. P. & Fitzallen, A. (2017). Site characterisation for the Ballina field testing facility. *Géotechnique* **67**, No. 4, 279–300, https://doi.org/10.1680/jgeot.15.P.211.

Lehane, B., Schneider, J. & Xu, X. (2005). The UWA-05 method for prediction of axial capacity of driven piles in sand. In *Frontiers in offshore geotechnics* (eds M. J. Cassidy and S. Gourvenec), pp. 683–689. Leiden, the Netherlands: CRC Press (Balkema).

Li, L., Li, J., Huang, J. & Gao, F. P. (2017). Bearing capacity of spudcan foundations in a spatially varying clayey seabed. *Ocean Engng* **143**, 97–105.

Liu, Y., Lee, F. H., Quek, S. T. & Beer, M. (2014). Modified linear estimation method for generating multi-dimensional multi-variate Gaussian field in modelling material properties. *Probabilist. Engng Mech.* **38**, 42–53.

Liyanapathirana, D. S. (2009). Arbitrary Lagrangian Eulerian based finite element analysis of cone penetration in soft clay. *Comput. Geotech.* **36**, No. 5, 851–860.

Low, H. E., Lunne, T., Andersen, K. H., Sjursen, M. A., Li, X. & Randolph, M. F. (2010). Estimation of intact and remoulded undrained shear strengths from penetration tests in soft clays. *Géotechnique* **60**, No. 11, 843–859, https://doi.org/10.1680/geot.9.P.017.

Lu, Q., Randolph, M. F., Hu, Y. & Bugarski, I. (2004). A numerical study of cone penetration in clay. *Géotechnique* **54**, No. 4, 257–267, https://doi.org/10.1680/geot.2004.54.4.257.

Lunne, T. (2012). The Fourth James K. Mitchell Lecture: the CPT in offshore soil investigations – a historic perspective. *Geomech. Geoengng* **7**, No. 2, 75–101.

Lunne, T., Robertson, P. K. & Powell, J. J. M. (1997). *Cone penetration testing in geotechnical engineering practice*. New York, NY, USA: Blackie Academic and Professional.

Ma, H., Zhou, M., Hu, Y. & Hossain, M. S. (2016). Interpretation of layer boundaries and shear strengths for soft-stiff-soft clays using CPT data: LDFE analyses. *J. Geotech. Geoenviron. Engng* **142**, No. 1, 04015055.

Matsuo, M. (1976). *Reliability in embankment design*. Cambridge, MA, USA: MIT, Department of Civil Engineering.

Pan, Y., Liu, Y., Lee, F. H. & Phoon, K. K. (2019). Analysis of cement-treated soil slab for deep excavation support–a rational approach. *Géotechnique* **69**, No. 10, 888–905, https://doi.org/10.1680/jgeot.18.P.002.

Pan, Y., Liu, Y., Tyagi, A., Lee, F. H. & Li, D. Q. (2020). Model-independent strength-reduction factor for effect of spatial variability on tunnel with improved soil surrounds. *Géotechnique*, https://doi.org/10.1680/jgeot.19.P.056.

Phoon, K. K. & Kulhawy, F. H. (1999). Characterization of geotechnical variability. *Can. Geotech. J.* **36**, No. 4, 612–624.

Phoon, K. K., Quek, S. T., Chow, Y. K. & Lee, S. L. (1990). Reliability analysis of pile settlement. *J. Geotech. Engng* **116**, No. 11, 1717–1734.

Randolph, M. F. & Gourvenec, S. (2011). *Offshore geotechnical engineering*. London, UK: Spon Press.

Robertson, P. K. (1990). Soil classification using the cone penetration test. *Can. Geotech. J.* **27**, No. 1, 151–158.

Robertson, P. K., Davies, M. P. & Campanella, R. G. (1989). Design of laterally loaded driven piles using the flat dilatometer. *Geotech. Test. J.* **12**, No. 1, 30–38.

Ronold, K. O. (1990). Random field modeling of foundation failure modes. *J. Geotech. Engng* **116**, No. 4, 554–570.

Sanglerat, G. (1972). *The penetrometers and soil exploration*. Amsterdam, the Netherlands: Elsevier.

Shi, G., Pan, Y., Sun, Z., Liu, Y. & Lee, F. H. (2020). Characteristic strength of soils underlying foundations considering effect of spatial variability. *Can. Geotech. J.* **57**, No. 4, 518–536.

Tabarroki, M. & Ching, J. (2019). Discretization error in the random finite element method for spatially variable undrained shear strength. *Comput. Geotech.* **105**, 183–194.

Teh, C. I. & Houlsby, G. T. (1991). An analytical study of the cone penetration test in clay. *Géotechnique* **41**, No. 1, 17–34, https://doi.org/10.1680/geot.1991.41.1.17.

Uzielli, M., Vannucchi, G. & Phoon, K. K. (2005). Random field characterisation of stress-normalised cone penetration testing parameters. *Géotechnique* **55**, No. 1, 3–20, https://doi.org/10.1680/geot.2005.55.1.3.

Van Dijk, B. F. J. & Kolk, H. J. (2010). CPT-based design method for axial capacity of offshore piles in clays. In *Frontiers in offshore geotechnics II* (eds S. Gourvenec and D. White), pp. 555–560. Boca Raton, FL, USA: CRC Press.

Vanmarcke, E. H. (1977). Probabilistic modeling of soil profiles. *J. Geotech. Engng Div.* **103**, No. 11, 1227–1246.

Walker, J. & Yu, H. S. (2010). Analysis of the cone penetration test in layered clay. *Géotechnique* **60**, No. 12, 939–948, https://doi.org/10.1680/geot.7.00153.

Wang, D., Hu, Y. & Randolph, M. F. (2010). Three-dimensional large deformation finite element analysis of plate anchors in uniform clay. *J. Geotech. Geoenviron. Engng* **136**, No. 2, 355–365.

Wang, D., Bienen, B., Nazem, M., Tian, Y., Zheng, J., Pucker, T. & Randolph, M. (2015). Large deformation finite element analyses in geotechnical engineering. *Comput. Geotech.* **65**, 104–114.

Xie, G. H. (2009). *Stochastic analysis of geotechnical parameters and study on stable reliability of slope*. Changsha, China: Central South University.

Yan, S. W., Zhu, H. X. & Liu, R. (2009). Numerical studies and statistic analyses of correlation distances of soil properties in Tianjin Port. *Rock and Soil Mechanics* **30**, No. 7, 2179–2185.

Yi, J., Huang, L. Y., Li, D. Q. & Liu, Y. (2020). A large-deformation random finite-element study: failure mechanism and bearing capacity of spudcan in a spatially varying clayey seabed. *Géotechnique* **70**, No. 5, 392–405, https://doi.org/10.1680/jgeot.18.P.171.

Yu, H. S. (2000). *Cavity expansion methods in geomechanics*. Dordrecht, the Netherlands: Springer Science Business Media.

Zhang, W., Wang, D., Randolph, M. F. & Puzrin, A. M. (2015). Catastrophic failure in planar landslides with a fully softened weak zone. *Géotechnique* **65**, No. 9, 755–769, https://doi.org/10.1680/geot14.P.218.

Zhou, M., Hossain, M. S., Hu, Y. & Liu, H. (2013). Behaviour of ball penetrometer in uniform single- and double-layer clays. *Géotechnique* **63**, No. 8, 682–694, https://doi.org/10.1680/geot.12.P.026.

Zhu, D., Griffiths, D. V. & Fenton, G. A. (2019). Worst-case spatial correlation length in reliability analysis of excavated clay slopes. In *Proceedings of the 7th international symposium on geotechnical safety and risk* (eds J. Ching, D. Li and J. Zhang), pp. 273–278. Singapore: Research Publishing.

Downloaded by [Universitetsbiblioteket i Trondheim] on [25/08/20]. Copyright © ICE Publishing, all rights reserved.